


Structural and optical properties of Ag doped tungsten oxide (WO₃) by microwave-assisted chemical route

S. Mohammed Harshulkhan¹  · K. Janaki² · G. Velraj³ · R. Sakthi Ganapathy¹ · S. Krishnaraj¹

Received: 23 October 2015 / Accepted: 7 November 2015 / Published online: 19 December 2015
© Springer Science+Business Media New York 2015

Abstract The present study explores, the pure and silver (Ag) doped WO₃ nanoparticles synthesized by microwave irradiation method. Powder X-ray diffraction results reveal that the WO₃ doped with Ag concentration from 0 to 10 wt% crystallizes in monoclinic structure. TEM analysis shows both pristine and silver doped WO₃ nanoparticles. They are having spherical morphology with a average size from 30 to 40 nm. Scanning electron microscopy studies depicts that both the pristine and Ag doped WO₃ form in spherical shaped morphology with an average diameter of 40–30 nm, which is in proper agreement with the average crystallite sizes calculated by Scherrer's formula. A considerable red shift in the absorbing band edge and a decrease in the band gap energy from 3.00 to 2.85 eV for Ag doped samples were observed by using UV–DRS spectra analysis. The defects in crystal and oxygen deficiencies were analyzed by photoluminescence spectra analysis.

1 Introduction

In the recent years, photocatalytic technology has received universal attention due to its application in organic synthesis and the abatement of pollutants in water and air. It is

used to remove the organic pollutant which includes detergent, dyes, pesticides and herbicides under UV-light irradiation. The heterogeneous photocatalysis attracted a considerable attention due to elimination of organic pollutants in water [1–4] and Semiconductor photocatalysts drew attention due to low cost and environmental friendliness. Because of its low cost and stability towards corrosion, TiO₂ is used as commercial photocatalytic material which has bandgap energy of 3.2 eV and it will be excited by UV irradiation and limits further application in the visible light region.

Transition metal oxides represent a large family of materials possessing various interesting properties such as colossal magneto-resistance, piezoelectricity and superconductivity. Among them, tungsten oxide is an n-type semiconductor metal oxide material which has its band gap in the range of 2.6–3.0 eV and it can be irradiated by visible light [5]. Since, the tungsten metal has several oxidation numbers, tungsten oxide forms different compounds such as W₃O, WO₂, WO_{2.72}, WO_{2.9}, WO_{2.96} and WO₃ [6]. Tungsten oxide shows several outstanding properties like electrochromic [7], gaschromic [8], photochromic [9], gas sensor [10], photocatalyst [11] and photoluminescence properties [12]. Tungsten oxide is prepared by various methods like sol–gel method, Chemical precipitation method, hydrothermal process, sputtering technique and microwave irradiation method. Among these methods microwave irradiation method is very simple due to its operation, less consumption of time, and purity of the material when compared to other methods [13].

The photocatalytic performances of WO₃ were studied for several additives and dopants. To modify the electronic structure and their surface properties of semiconductor, the chemical doping of WO₃ with metallic elements are used extending their visible light absorbance. When compared to

✉ S. Mohammed Harshulkhan
harshulkhan21@gmail.com

¹ Vinayaka Mission's Kirupananda Variyar Engineering College, Salem 636308, TN, India

² Government Arts College for Women, Salem 636008, TN, India

³ Department of Physics, Anna University, Chennai 600025, TN, India

other transition metals, Ag plays a vital role in the enhancement of photocatalytic activity of WO_3 . Cong and Lin [14] have successfully prepared Eu^{3+} doped WO_3 nanoparticles by the modified method of Pechini. The photocatalytic activities of the nanoparticles were evaluated by photodecomposition of rhodamine B (rhB). The result indicates that the Eu^{3+} doped WO_3 nanoparticles exhibit the highest photocatalytic activity. In the recent study, it has been reported that the tungsten oxide synthesis was found along with the water molecule ($\text{WO}_3 \cdot \text{H}_2\text{O}$) by microwave irradiation method [15]. In the present research the pure and silver doped Tungsten oxide without hydrate group were synthesized by microwave irradiation method. For the first time the study yielded the pure and silver doped tungsten oxide directly from the microwave Irradiation method without hydrate group (H_2O). In both the cases, the time taken to complete the synthesis was around 5 min and the reaction process is very simple.

2 Experimental procedure

2.1 Material preparation

The precursor solution is prepared by adding tungstic acid in 10 ml of sodium hydroxide (NaOH) solution which results in an yellow colour solution due to proton exchange protocol process. Again hydrochloric acid (HCl) is added drop by drop till it attains pH value 1. Hydrochloric acid acts as a precipitating agent and also as the medium for the required product to have desired morphology [16]. After accomplishing the pH value, 5 ml of distilled water is added for immediate response of microwave with precursor solution. Eventually the solution was placed into the Microwave oven (2.45 GHz) under optimum power of 360 W for 5 min in air atmosphere. After the irradiation process, the resulted substance was dried in convection mode at 100 °C for 5 min. The silver doped WO_3 was synthesized by adding tungstic acid and silver nitrate at molar ratio (0.03 and 0.10) in 10 ml of sodium hydroxide (NaOH) solution. The above procedure was repeated to obtain the final product. The final product was pale green in colour for pure WO_3 and Ag doped WO_3 .

2.2 Characterization techniques

The surface morphology, structural and chemical state of the obtained Nanomaterial was characterized by using X-ray diffraction method (X-ray Diffractometer-XPRT PRO). Transmission electron microscope and selected-area electron diffraction was recorded with JEM2100. High resolution electron microscope was recorded with an accelerating voltage of 200 kV. Optical measurements were carried out in UV–Vis spectroscopy (SHIMADZU 3600 UV–Vis

spectrometer), Surface morphology was studied by scanning electron microscopy (FEIQUATA250), Elemental analysis were performed by EDAX (FEIQUATA250) and PL spectra was recorded by LS 45 fluorescence spectrometer.

3 Results and discussion

3.1 XRD analysis

The microstructure of the prepared samples were analysed by X-ray diffraction (XPRT PRO) using the Cu $K\alpha$ wavelength of 1.5405 Å. The average crystalline size and structures were calculated from X-ray diffraction pattern which is shown in Fig. 1. The XRD pattern of the sample shows the formation of WO_3 and diffractions matched perfectly with the WO_3 monoclinic structure [17]. Figure 1 shows the X-ray diffraction (XRD) pattern for synthesized pure and Ag doped WO_3 . From the figure it has been observed that the Pure WO_3 exhibit the diffraction peak at $2\theta = 23.123, 23.594$ and 24.371 and for Ag doped WO_3 exhibits the diffraction peak at $2\theta = 23.024, 23.498$ and 24.270 related to (002), (020), (200) reflection of monoclinic phase of WO_3 . Both Ag doped WO_3 and undoped WO_3 can be well indexed to the standard pattern of monoclinic WO_3 with the lattice constants $a = 7.300$, $b = 7.538$, $c = 7.689$ and $\beta = 90.892$ (JCPDS card No: 83-0950). No additional peaks are found in the XRD pattern which confirms absence of impurities in the synthesized material. It was also noted that the small peak shift was observed for lower angle side for Ag doped samples. Moreover, the intensity of the peak decreases with the increase in the Ag concentrations. These results clearly indicate that Ag substituted in WO_3 host lattice site.

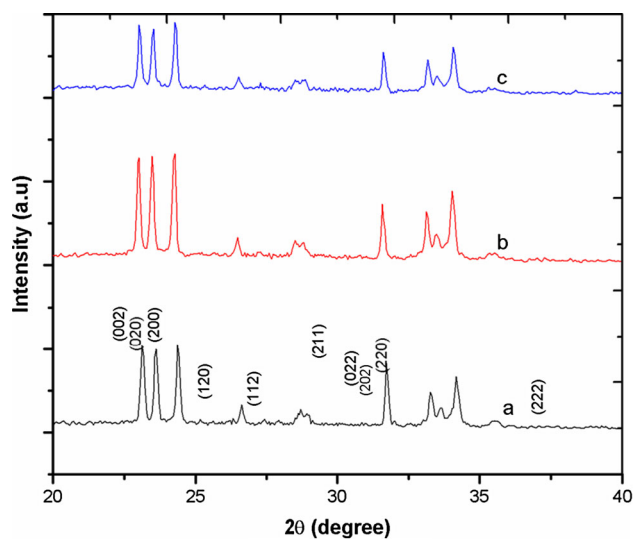


Fig. 1 XRD pattern for a Pure WO_3 , b 3 wt% Ag, c 10 wt% Ag

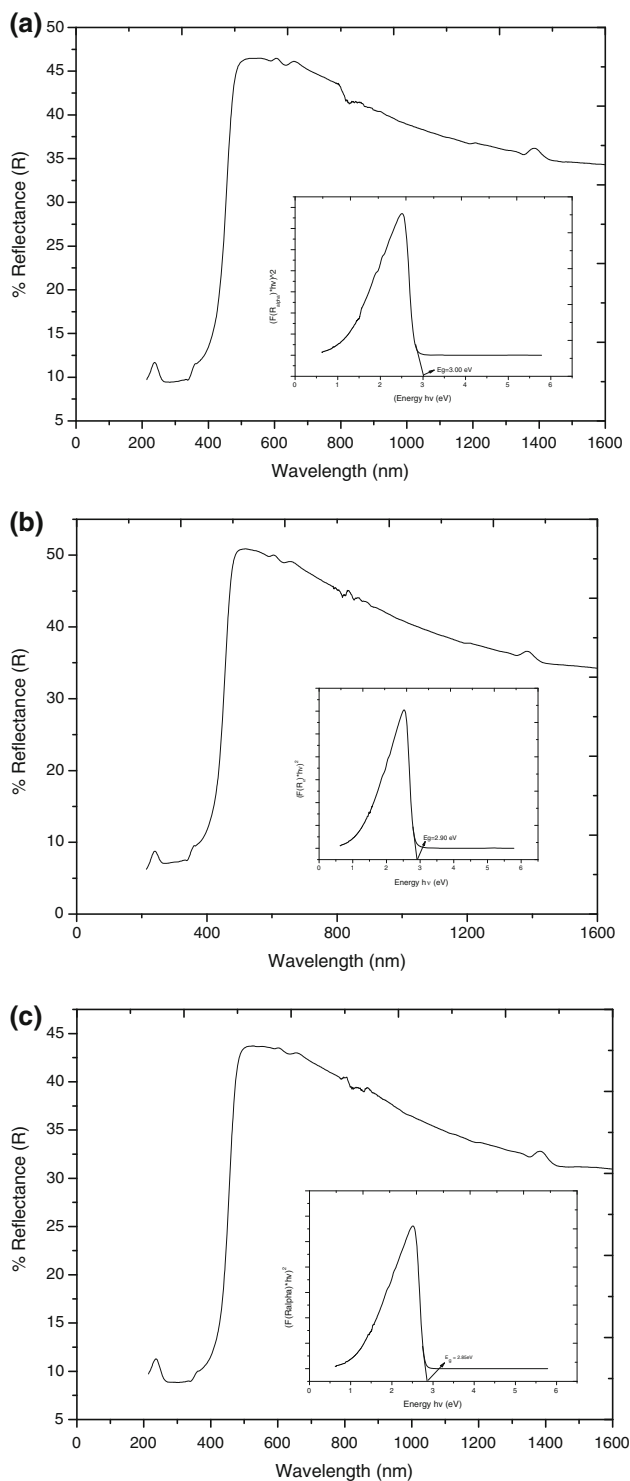


Fig. 2 **a** UV–visible DRS spectra for Pure WO_3 . **b** UV–visible DRS spectra for 3 wt% Ag doped WO_3 . **c** UV–visible DRS spectra for 10 wt% Ag doped WO_3

By using the Debye–scherrer’s equation [18, 19], the average grain size are calculated based on the peaks found in the XRD pattern from $2\theta = 23^\circ$ to 25° . The crystalline

size (D) of the pure and Ag doped WO_3 were calculated by using Debye–Scherrer’s relation,

$$D = \frac{0.9\lambda}{\beta \cos \theta} \text{ nm}$$

where β is the full width at half maximum, λ is the X-ray wavelength (0.15406 nm), and θ is the diffraction angle. The average crystallite size is calculated for pure WO_3 is 35 and 33 nm, 31 nm for 3 and 10 % of Ag doped WO_3 . The average crystallite size of pristine WO_3 was found to be 35 nm and it was further decreased to 31 nm for 10 wt% Ag doped WO_3 . The XRD results reveal that the crystalline size has decreased with increase in Ag concentration.

3.2 UV–visible diffusion reflectance spectroscopy

The optical property and substitution of silver into WO_3 site, the sample were characterized by UV–Vis transmission spectra analysis. Figure 2a, b shows the diffusion reflectance spectra of pure and Ag doped WO_3 respectively. It was observed that the optical transparency of the pure WO_3 decreases with increase in the Ag content. The decrease in the transparency of Ag doped WO_3 was attributed to the increase in reflectance due to the presence of the metal ion. A considerable red shift was observed in the absorption edges with the increase of Ag content from 0 to 10 wt%, which indicates the decrease in bandgap of WO_3 on doping. The band gap energies (E_g) have been calculated using Kubelka–Munk (K–M) model as described below. The K–M model [20] at any wavelength is given by

$$\frac{K}{S} = \frac{(1 - R_\infty)^2}{2R_\infty} = F(R_\infty)$$

$F(R_\infty)$ is the so called remission or Kubelka–Munk function, where

$$(R_\infty) = \frac{R_{\text{sample}}}{R_{\text{standard}}}$$

A graph is plotted between $[F(R_\infty)hv]^2$ versus hv and the intercept value gives the band gap energy E_g [15] of the individual sample. The band gap energies were calculated for pure and 3, 10 wt% Ag doped WO_3 are tabulated. These values offer an excellent agreement with the reported value. Table 1 shows the bandgap energy for pure and Ag doped WO_3 .

Table 1 Band gap energy for pure and Ag doped WO_3

| Material | Bandgap energy (eV) |
|--------------------|---------------------|
| Pure WO_3 | 3.00 |
| 3 wt% Ag | 2.94 |
| 10 wt% Ag | 2.85 |

3.3 Scanning electron microscopy and EDAX analysis

Scanning electron microscope is a useful technique to determine the morphology and particle size of the samples. Figure 3a and 4a shows SEM image of pure and Ag doped WO₃ nanoparticles. It is clearly observed that both the samples show plate like morphology with average diameter of 1–1.5 μm and thickness of 80–100 nm. The particle size estimated from XRD results much smaller than the SEM results. This change in size could be due to the larger particles which are composed of many smaller particles. After doping of Ag dopant the plate like morphology decreases when increasing the Ag content as shown in the Fig. 4a. The decrease of crystalline size was also confirmed by XRD results. The EDAX results confirm the obtained

materials which are composed of W and O as shown in the Fig. 3b. Figure 4b shows the EDAX spectra for silver doped WO₃ that confirms the presence of silver in the synthesized material. The intensity peak of tungsten was decreased due to the addition of silver ions in the tungsten site and intensity peak of oxygen remains constant for both pure and Ag doped WO₃.

3.4 Transmission electron microscope

Figure 5a, b shows the TEM image of both pristine and Ag doped WO₃ nanoparticles. It is clearly observed that both particle have spherical shaped morphology with an average diameter of about 30–40 nm for pure and Ag doped WO₃ nanoparticle which shows very good agreement with XRD result. The morphology of the doped particles remain

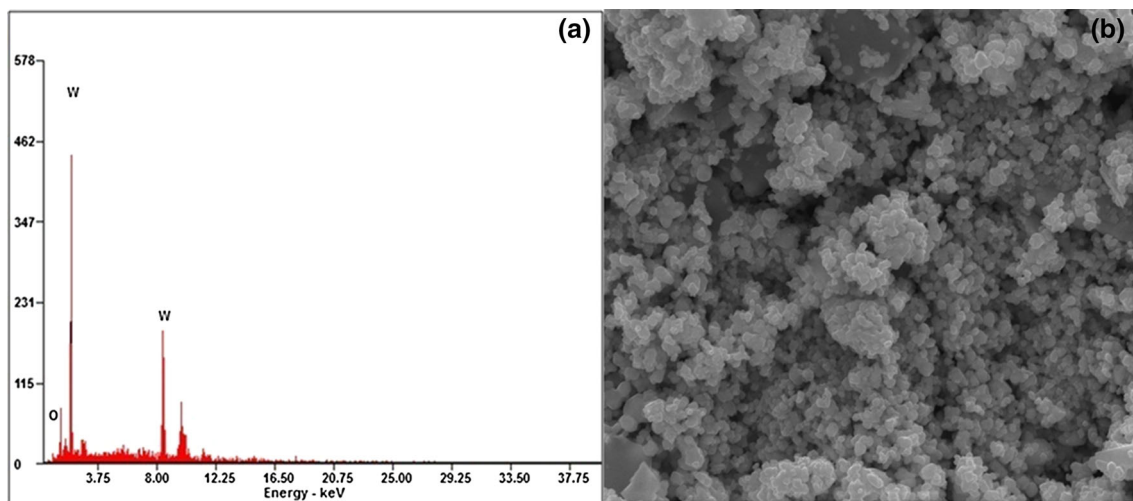


Fig. 3 a and b SEM and EDX spectra of WO₃

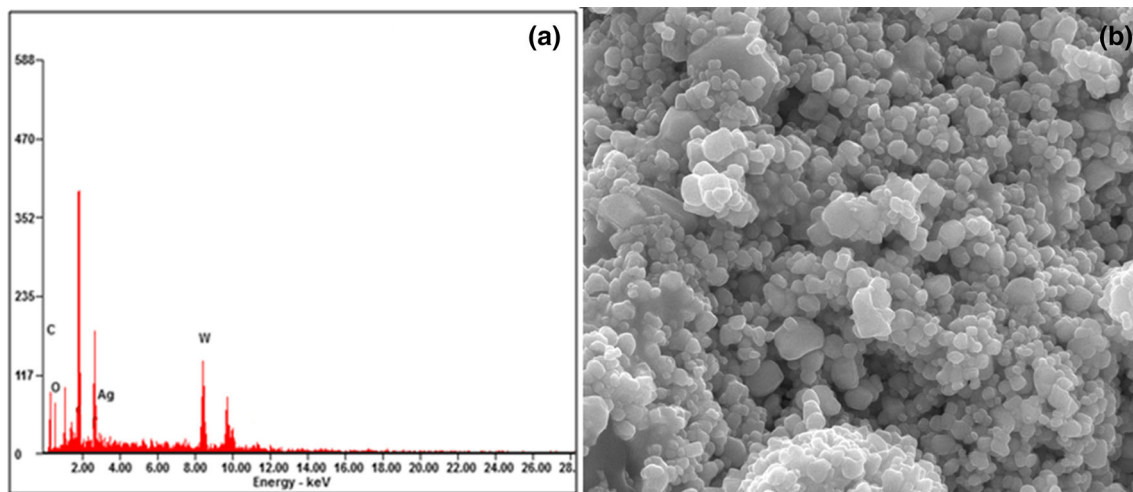


Fig. 4 a and b SEM and EDX spectra of Ag doped WO₃

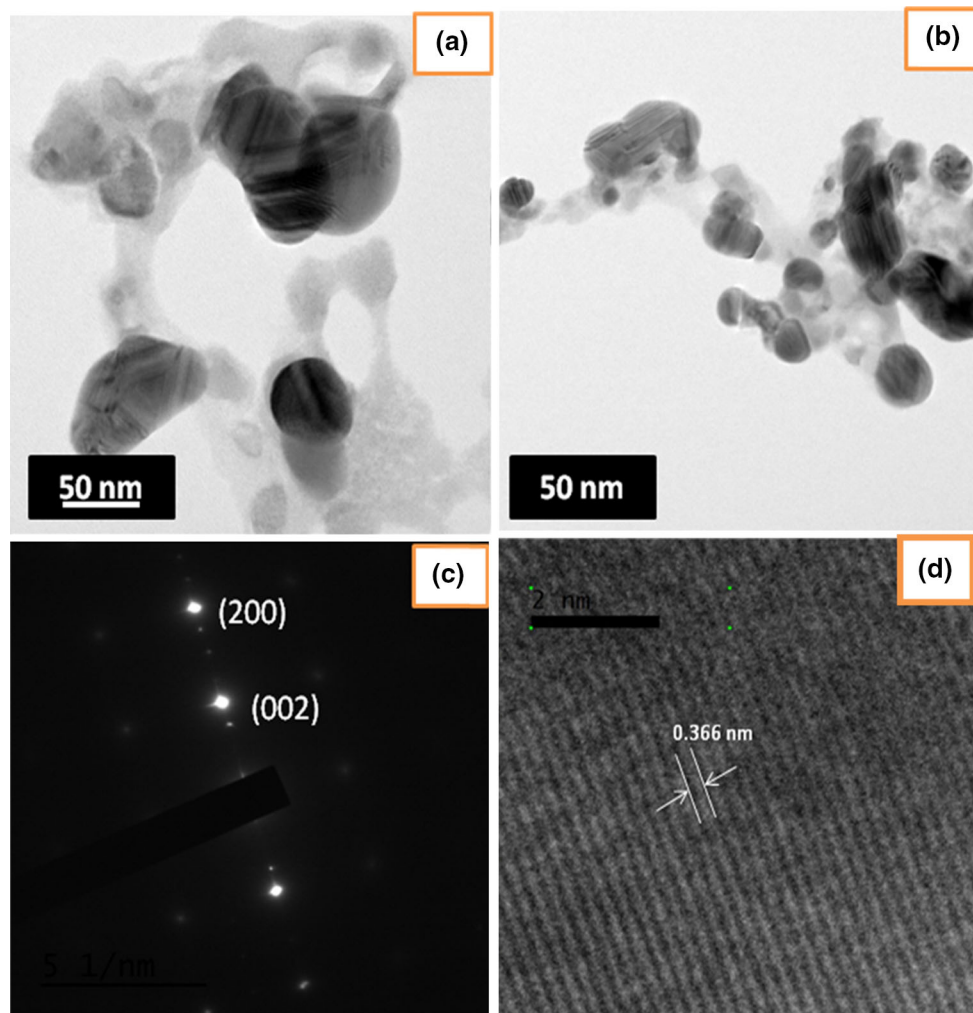


Fig. 5 TEM image of **a** Pure WO_3 , **b** 10 wt% Ag doped WO_3 , **c** SAED pattern of Ag doped WO_3 , **d** HRTEM image of Ag doped WO_3

unchanged but the average diameter got decreased. Figure 5c, d show the SAED pattern and HRTEM image of Ag doped WO_3 nanoparticles. The SAED pattern confirms that the prepared material is well crystallized nanoparticles grown along the [002] direction [21]. The HRTEM images show that the interplanar distance of Ag doped WO_3 is 0.366 nm for the crystal plane [002] [22].

3.5 Photoluminescence studies

The PL spectroscopy is a useful study to measure the energy distribution of emitted photons after optical excitation and to understand the electron hole pair in the semiconducting oxide materials [23]. The oxygen vacancy and lattice distortion of pure and silver doped tungsten oxide samples were analyzed using photoluminescence spectra and it is shown in the Fig. 6. The spectra were recorded under the excitation wavelength of 325 nm at room temperature. Both pure and Ag doped tungsten oxide

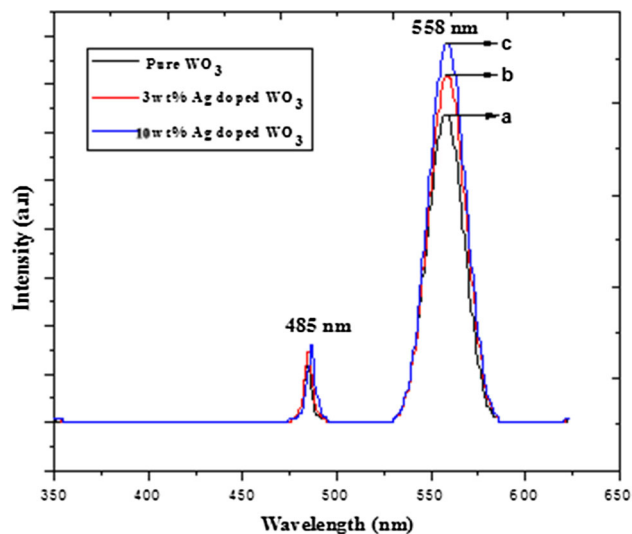


Fig. 6 Photoluminescence spectra for **a** pure WO_3 , **b** 3 wt% Ag, **c** 10 wt% Ag

material show blue emission (485 nm) and green emission (558 nm). The blue emission is due to the defect level in the bandgap for its electron transition. The green emission peak (558 nm) is related to v_o^+ oxygen vacancies and these emission may be attributed to the different luminescent centers such as defect energy levels arising due to silver interstitials and oxygen vacancies as well as dangling bonds into nanocrystals. Due to the silver doped into tungsten oxide, the intensity of peaks increases and shifted towards the higher energy. The increase in the peak intensity is due to the presence of Ag into WO_3 which causes the lattice defects.

4 Conclusion

Finally, it has been substantiated that a simple and inexpensive microwave irradiation method is used to synthesize the pure and Ag doped WO_3 . The crystalline size and structure were evaluated from XRD which has monoclinic structure and crystallite which ranges from 35 to 31 nm. TEM analysis shows both pristine and Ag doped WO_3 nanoparticles are spherical shaped morphology with average particle size from 40 to 30 nm and it was compared and in very good agreement with the XRD result. The UV–DRS method was used to calculate the bandgap energies of the prepared material and it has an effective with the reported value. The bandgap energy value shows the emission of radiation in the visible region. Ag doping into the WO_3 reduces the bandgap which is evident by a red shift in the optical absorption edge and that was found by UV–DRS method. Scanning electron microscopy confirms the plate like morphology change as the silver concentration increases in the WO_3 . The energy dispersive spectrum confirms the presence of tungsten, oxygen and silver in the synthesized materials. UV–DRS analysis shows that the band gap energy decreases with the increase in the particle size. The PL studies show the red shifts in the optical absorption edge and the same was obtained for pure and Ag doped WO_3 . The material can be excited by visible light and this property is used to remove the organic pollutant from the waste water.

Acknowledgments The author extends his gratitude to Dr. T. Shanthi, Mr. M. Nagarajan and Mrs. P. Rajini for their earnest motivation and abiding support. Author also thank Dr. M. Parthibavarman and Dr. P. Kanchana for their positive suggestions rendered during the research work.

References

1. S. Malato, P. Fernandez-Ibanez, M.I. Maldonado, J. Blanco, W. Gernjak, Recent overview and trends. *Catal. Today* **147**, 1–59 (2009)
2. M.A. Rauf, S.S. Ashraf, Fundamental principles and application of heterogeneous photocatalytic degradation of dyes in solution. *J. Chem. Eng.* **151**, 10–18 (2009)
3. A.R. Khataee, M.B. Kasiri, Photocatalytic degradation of organic dyes in the presence of nanostructured titanium dioxide: influence of the chemical structure of dyes. *J. Mol. Catal. A: Chem.* **328**, 8–26 (2010)
4. S. Ahmed, M.G. Rasul, W.N. Martens, R. Brown, M.A. Hashib, Advances in heterogeneous photocatalytic degradation of phenols and dyes in wastewater: a review. *Water Air Soil Pollut.* **215**, 3–29 (2011)
5. C.G. Granqvist, Electrochromic tungsten oxide films: review of progress 1993–1998. *Sol. Energy Mater. Sol. Cells* **60**, 201–262 (2000)
6. M. Gillet, K. Masek, E. Gillet, Structure of tungsten oxide nanoclusters. *Surf. Sci.* **566–568**, 383–389 (2004)
7. C.G. Granqvist, *Handbook of electrochromic materials* (Elsevier, Amsterdam, 1995)
8. S.H. Lee et al., Gasochromic mechanism in a- WO_3 thin films based on Raman spectroscopic studies. *J. Appl. Phys.* **88**, 3076–3078 (2000)
9. C.O. Avellaneda, L.O.S. Bulhoes, Intercalation in WO_3 and WO_3 : Li films. *Solid State Ionics* **165**, 59–64 (2003)
10. E. Gyorgy, G. Socol, I.N. Mihailescu, C. Ducu, S. Ciuca, Structural and optical characterization of WO_3 thin films for gas sensor applications. *J. Appl. Phys.* **97**, 093527–093527-4 (2005)
11. M. Feng et al., Strong photoluminescence of nanostructured crystalline tungsten oxide thin films. *Appl. Phys. Lett.* **86**, 141901–141903 (2005)
12. R. Aimirad, O. Akhavan, A.Z. Moshfegh, Influence of coloring voltage and thickness on electrochromical properties of e-beam evaporated WO_3 thin films. *J. Electrochem. Soc.* **153**, E11–E16 (2006)
13. M. Parthibavarman, K. Vallalperuman, S. Sathishkumar, M. Durairaj, K. Thavamani, A novel microwave synthesis of nanocrystalline SnO_2 and its structural optical and dielectric properties. *J. Mater. Sci.: Mater. Electron.* **25**, 730–735 (2014)
14. W. Cong, C.A.O. Lin, Preparation, spectral characteristics and photocatalytic activity of Eu^{3+} -doped WO_3 nanoparticles. *J. Rare Earths* **29**, 727–731 (2011)
15. V. Hariharan, M. Parthibavarman, C. Sekar, *J. Alloys Compd.* **509**, 4788–4792 (2011)
16. T. Jesionowski, Characterisation of silicas precipitated from solution of sodium metasilicate and hydrochloric acid in emulsion medium. *Powder Technol.* **127**, 56–65 (2002)
17. D. Sanchez-Martinez et al., Characterization and photocatalytic properties of hexagonal and monoclinic WO_3 prepared via microwave-assisted hydrothermal synthesis. *J. Mater. Res. Bull.* **48**, 691–697 (2013)
18. W.F. Zhang, M.S. Zhang, Z. Yin, Q. Chen, Photoluminescence in anatase titanium dioxide nanocrystals. *Q. Appl. Phys. B* **70**, 261–265 (2000)
19. R. Yousefi, B. Kamaluddin, Fabrication and characterization of ZnO and ZnMgO nanostructures grown using a ZnO/ZnMgO compound as the source material. *Appl. Surf. Sci.* **256**, 329–334 (2009)
20. A. EscobedoMorales, E. SanchezMora, U. Pal, Use of diffuse reflectance spectroscopy for optical characterization of un-supported nanostructures. *Rev. Mex. Fis.* **53**, 18–22 (2007)
21. Tomoharu Tokunaga, Tadashi Kawamoto, Kenta Tanaka, Yasuhiko Hayashi, Katsuhiko Sasaki, Kotaro Kuroda, Growth and structure analysis of tungsten oxide nanorods using environmental TEM. *Nanoscale Res. Lett.* **7**(1), 85 (2012)
22. W.H. Lai, J. Shieh, L.G. Teoh, M.H. Hon, Fabrication of one-dimensional mesoporous tungsten oxide. *Nanotechnology* **17**, 110–115 (2006)
23. Wu Ping, Qiang Li, Xingquan Zou, Wende Cheng, Danli Zhang, Chuanxi Zhao, Lingfei Chi, Tan Xiao, Correlation between photoluminescence and oxygen vacancies in In_2O_3 , SnO_2 and ZnO metal oxide nanostructures. *J. Phys: Conf. Ser.* **188**, 012054 (2009)